Systems/Circuits

Perceptual Weighting of V1 Spikes Revealed by Optogenetic White Noise Stimulation

Julian Day-Cooney, Jackson J. Cone, and John H. R. Maunsell
Department of Neurobiology and Neuroscience Institute, University of Chicago, Chicago, Illinois 60637

During visually guided behaviors, mere hundreds of milliseconds can elapse between a sensory input and its associated behavioral response. How spikes occurring at different times are integrated to drive perception and action remains poorly understood. We delivered random trains of optogenetic stimulation (white noise) to excite inhibitory interneurons in V1 of mice of both sexes while they performed a visual detection task. We then performed a reverse correlation analysis on the optogenetic stimuli to generate a neuronal-behavioral kernel, an unbiased, temporally precise estimate of how suppression of V1 spiking at different moments around the onset of a visual stimulus affects detection of that stimulus. Electrophysiological recordings enabled us to capture the effects of optogenetic stimuli on V1 responsivity and revealed that the earliest stimulus-evoked spikes are preferentially weighted for guiding behavior. These data demonstrate that white noise optogenetic stimulation is a powerful tool for understanding how patterns of spiking in neuronal populations are decoded in generating perception and action.

Key words: **detection; optogenetics; perception; V1; visual cortex; white noise**

Significance Statement

During visually guided actions, continuous chains of neurons connect our retinas to our motoneurons. To unravel circuit contributions to behavior, it is crucial to establish the relative functional position(s) that different neural structures occupy in processing and relaying the signals that support rapid, precise responses. To address this question, we randomly inhibited activity in mouse V1 throughout the stimulus-response cycle while the animals did many repetitions of a visual task. The period that led to impaired performance corresponded to the earliest stimulus-driven response in V1, with no effect of inhibition immediately before or during late stages of the stimulus-driven response. This approach offers experimenters a powerful method for uncovering the temporal weighting of spikes from stimulus to response.

Introduction

How neuronal sensory signals are decoded to generate perceptions and guide behavior remains a central question in neuroscience. Quantitative measures of the relationships between sensory stimuli, population spiking, and behavior have been instrumental in guiding thinking on this subject. Measurements of correlations between neuronal responses and perceptual reports (choice probability; Parker and Newsome, 1998; Gold and Shadlen, 2007; Nienborg and Cumming, 2009; Nienborg et al., 2012) or correlations between neuronal response latencies and reaction times (Seal et al., 1983; DiCarlo and Maunsell, 2005; Lee et al., 2016) have provided insights about which neurons are likely to contribute to a behavior, but correlative approaches require comprehensive assessment of noise correlations within large populations to determine which signals actually contribute to a behavior (Haefner et al., 2013). Ultimately, perturbations of circuit activity are necessary to establish causal relationships.

Perturbing the activity of neuronal populations with electrical microstimulation or pharmacological agents has long been used to provide direct evidence of causal relationships between neuronal spiking and behavior (Histed et al., 2013; Wurtz, 2015). Optogenetic techniques have advanced circuit perturbation experiments by making it possible to selectively modulate the spiking of genetically defined cell types with temporal precision in the range of milliseconds (Bernstein and Boyden, 2011). However, most studies that use optogenetics to modulate spiking in behaving animals have delivered stimulation lasting hundreds of milliseconds or longer (Lee et al., 2012; Glickfeld et al., 2013; Guo et al., 2014; Goard et al., 2016; Cone et al., 2020). Extended perturbations provide valuable insights, but to understand how

Received Aug. 26, 2021; revised Jan. 17, 2022; accepted Jan. 19, 2022.

Author contributions: J.D.-C., J.J.C., and J.H.R.M. designed research; J.D.-C. and J.J.C. performed research; J.D.-C., J.J.C., and J.H.R.M. analyzed data; J.D.-C., J.J.C., and J.H.R.M. wrote the paper.

This work was supported by National Institutes of Health Grants U19 NS107464 (J.H.R.M.) and R21EY032650 (J.H.R.M. and J.J.C.), and a postdoctoral fellowship from the Arnold and Mabel Beckman Foundation (J.J.C.). We thank Dr. Supriya Ghosh, Dr. Nicolas Masse, and Matthew Rosen for comments on drafts of this manuscript.

J. Day-Cooney's present address: Vollum Institute, Oregon Health & Science University, Portland, Oregon.

The authors declare no competing financial interests.

Correspondence should be addressed to John H. R. Maunsell at maunsell@uchicago.edu.

https://doi.org/10.1523/JNEUROSCI.1736-21.2022

different neurons contribute to a behavior, it is important to know how the behavioral impact of the spiking of different neurons varies moment to moment over the natural time course for initiating a response, which for many behaviors involves only 100–200 ms (Histed et al., 2012; Sachidhanandam et al., 2013).

Knowing how the spikes of specific neurons are weighted as a function of time during the generation of a response can reveal their relative significance to that behavior and their functional relationships to other contributing neurons. For example, Resulaj et al. (2018) varied the onset of a sustained optogenetic inhibition of mouse V1 neurons in 40 ms steps after the appearance of a visual stimulus and found that the first 80–100 ms of stimulus-evoked V1 activity is much more important for visual behaviors than subsequent V1 spiking. Modeling studies have suggested that the contributions of individual sensory neurons to perceptual decisions might be limited to substantially shorter intervals (Panzeri et al., 2001; VanRullen and Thorpe, 2002; Kirchner and Thorpe, 2006; Liu et al., 2009; Tchumatchenko et al., 2011; Shriki et al., 2012).

Optogenetic perturbations can be brief enough to probe neuronal contributions with high temporal resolution (<10 ms; Tchumatchenko et al., 2013), but delivering an isolated brief perturbation that is powerful enough to measurably alter behavior poses problems. Strong perturbations can produce long-lasting disruptions of circuit function, or they can serve as an alerting signal that alters behavioral state, in either case precluding assessments of time-restricted effects. Weaker brief perturbations can avoid these issues but are inefficient because many trials are needed to precisely estimate the modest behavioral effects of a weak perturbation, and many time offsets must be tested to densely sample the relevant interval with good temporal resolution.

These limitations can be overcome using the method of reverse correlation (De Boer and Kuyper, 1968). Reverse correlation using white noise stimuli has long been used as a highly efficient way to measure spatiotemporal receptive fields of sensory neurons (i.e., the stimulus-neuronal relationship; Eggermont et al., 1983; DiCarlo et al., 1998; Neri and Heeger, 2002; Schwartz et al., 2006). Reverse correlation has also been used to examine the relationship between sensory stimuli and behavioral reports, revealing which periods of sensory stimulation dominate in behavioral responses (the stimulus-behavioral relationship; Nienborg and Cumming, 2009; Okazawa et al., 2018). Here, we describe experiments in which we extended this approach by using white noise optogenetic stimulation of parvalbumin-expressing interneurons, which potently and quickly inhibit local principal neurons (Packer and Yuste, 2011), to reveal the temporal weighting of their spiking in generating a behavioral response (the neuronal-behavioral relationship). The results show that measurements of neuronal-behavioral kernels can provide a highly efficient approach to obtain spike weighting functions with high temporal resolution. They reveal that only very brief, stimulus-dependent epochs of V1 stimulus responses contribute to behavioral detection of visual stimuli.

Materials and Methods

Animal preparation

All animal procedures followed National Institutes of Health guidelines and were approved by the Institutional Animal Care and Use Committee of the University of Chicago. We used 28 mice (11 female) that were heterozygous for Cre recombinase in *Parvalbumin* (PV)-expressing cells, which provides a targeting specificity of ~93% (Pfeffer et al., 2013). Animals were outbred by crossing homozygous Cre-expressing PV-Cre mice (stock #017320, The Jackson Laboratory; Hippenmeyer et al., 2005) with wild-type BALB/c mice (stock #000651, The Jackson Laboratory). Animals were singly housed on a reverse light/dark cycle with *ad libitum* access to food. Mice were water scheduled throughout behavioral experiments, except for periods around surgeries.

Mice (3–5 months old) were implanted with a headpost and cranial window over V1 to give stable access for photostimulation during behavior (Goldey et al., 2014; Histed and Maunsell, 2014). For surgery, animals were anesthetized with isoflurane (induction, 3%; maintenance 1.0–1.5%) and given ketamine (40 mg/kg, i.p.) and xylazine (2 mg/kg, i.p.). Body temperature was maintained with a heating pad. A titanium headpost was secured to the skull with acrylic (C&B Metabond, Parkell) using aseptic technique. A craniotomy was made over V1 in the left cerebral hemisphere (3.0 mm lateral and 0.5 mm anterior to lambda) and covered with a glass window (3.0 mm diameter, 0.8 mm thick; Tower Optical). Mice were given analgesics postoperatively (buprenorphine, 0.1 mg/kg, and meloxicam, 2 mg/kg, i.p.).

After each animal had recovered from surgery, we located V1 by measuring changes in intrinsic autofluorescence using visual stimuli and epifluorescence imaging (Andermann et al., 2011). Autofluorescence produced by blue excitation (470 ± 40 nm, Chroma) was captured using a long-pass filter (500 nm cutoff), a 1.0× air objective (StereoDiscovery V8 microscope; ~0.11 NA, Zeiss) and a CCD camera (AxioCam MRm, Zeiss; 460 × 344 pixels; 4 × 3 mm FOV). The visual stimuli were full contrast drifting sinusoidally modulated luminance gratings appearing through a two-dimensional Gaussian aperture (Gabors). Gabor stimuli (10° SD; 30°/s; 0.1 cycles/degree) were presented for 10 s followed by 6 s of mean luminance at one of five visual field locations. The response to each visual stimulus was computed as the fractional change in fluorescence during the first 8 s of the stimulus presentation relative to the last 4 s of the preceding blank.

Virus injections were targeted to the monocular region of V1 based on the retinotopic map of each animal (25° azimuth; ±15° elevation). Mice were anesthetized (isoflurane, 1%–1.5%), their headpost was secured, and the cranial window was removed using aseptic technique. We used a volume injection system (UMC4, World Precision Instruments) to inject 200–400 nl of AAV9-Flex-ChR2-tdTomato (~10^{11} viral particles; Penn Vector Core) 250–400 µm below the cortical surface (50 nl/min). Following the injection, a new cranial window was sealed in place. Two to 3 weeks after injection, we localized the area of ChR2 expression using tdTomato fluorescence and attached an optical fiber (400 µm diameter; 0.48 NA; Doric Lenses) within 500 µm of the cranial window (~1.3 mm above the cortex).

Experimental design and statistical analysis

Behavioral task. Mice were trained to use a lever to respond to changes in a visual display for a water reward (Histed et al., 2012). During behavioral sessions, mice lay in a sled with their head fixed. Mice were positioned in front of a calibrated visual display that presented a uniform gray field. Mice self-initiated trials by depressing the lever, and a neutral tone indicated the start of each trial. The prestimulus period was randomly drawn from a uniform distribution (500–3000 ms), after which a static achromatic, odd-symmetric Gabor stimulus (5° SD, 0.1 cycles/degree) appeared. Mice had to release the lever within 100–700 ms after stimulus onset to receive a liquid reward (1.5–4 µl). Trials in which mice failed to release the lever within the response window resulted in a brief time out (1500–2500 ms). Trials in which mice released the lever before the onset of visual stimuli were unrewarded and excluded from analyses. Task parameters were slowly adjusted over several weeks until mice responded reliably to Gabor stimuli spanning a range of contrasts in the location of the V1 retinotopic map where optogenetic stimulation would be delivered during testing sessions [>60% hit rate for a range of stimulus contrasts, >300 trials a day; median training time: 61 d; interquartile range (IQR): 48–62 d]. For sessions with contrast ramps, the same Gabor (5° SD, 0.1 cycles/degree) appeared, but the contrast increased linearly from 0% to ~100% over 500 ms.

Behavioral analysis. In each daily session, mice were typically allowed to do a few dozen trials to stabilize their performance before trials with optogenetic stimulation were introduced. Only trials between the first and last trials with optogenetic stimulation were included in the analyses.

Although the percentage of successful lever releases provides a ready index of animal performance, it fails to account for successful guesses. The d′ measure from signal detection theory (Green and Swets, 1966) takes guesses into account and provides a more complete measure of the detection abilities of the animal. Calculation of d′ is based on a hit rate and a false alarm rate. Because false alarm rate is not directly available from trial outcomes in the visual detection task, we estimated that rate for each session by dividing the total trial time available for early lever releases by the number of early releases. The trial time available for early releases included the trial time before each early release and the time before each stimulus presentation on other trials (accounting for the ~100 ms period after stimulus onset during which responses were considered early because they were too fast to be valid). This rate of early lever releases was multiplied by the duration of the response window to obtain the probability of a false alarm. This false alarm probability was then used to convert the raw hit rate to a true hit rate by removing the fraction of hits attributable to spontaneous lever releases during the response window (false hits). A d′ value was computed separately for trials with and without optogenetic stimulation for each session. Because the rate of early lever releases was indistinguishable between stimulated and unstimulated trials ($p > 0.6$, paired t test), we used the combined false alarm rate in computing d′ for stimulated and unstimulated trials.

Optogenetic stimulation and analysis. Behavioral sessions with optogenetic stimulation began >4 weeks after ChR2 injection. Light was delivered through the optic fiber using a power-calibrated LED source (455 nm; Thorlabs). To prevent mice from seeing optogenetic stimuli, we enclosed the fiber implant in blackout fabric (Thorlabs) attached to the headpost using a custom mount. The timing of the optogenetic stimulus delivered on each trial was aligned with that of the visual stimulus using a photodiode mounted on the video display.

In some experiments, brief individual pulses of optogenetic stimulation were delivered before or after the onset of the visual stimulus (see Fig. 2; 11 mice, 6 female). The data presented were limited to sessions using pulses ≥0.25 mW and ≤100 ms. Median pulse power was 2.0 mW (1.0–2.5 IQR), median duration was 10 ms (5–20 IQR), and the median energy in the pulse was 20 μJ (5–50 IQR).

During other experiments using white noise optogenetic stimulation, the stimulus was delivered throughout each trial. To avoid an abrupt onset, the power of the optogenetic stimulus ramped up to the average mean power over the first 250 ms of the trial. That period was excluded from analysis. In preliminary sessions, the optogenetic stimulus for each animal was adjusted by presenting a constant stimulus power throughout trials. These sessions were used to set a power that produced an ~5–10% decrease in the proportion of correct trials, which was then used as the mean power in subsequent testing sessions. The required power varied between mice (median: 0.15 mW, IQR 0.09–0.25 mW), likely because of differences in the strength and spatial distribution of virus expression, optic fiber alignment, and behavioral capacity. Preliminary sessions used to determine stimulation powers were not included in analyses.

For trials with optogenetic stimulation, binary white noise optogenetic stimuli were generated by randomly assigning zero or maximum (2× mean) power to a series of 25 ms bins with equal probability. The resulting optogenetic stimulus produced equal power across all frequencies represented and is, therefore, a quasi white noise stimulus (Marmarelis and Marmarelis, 1978). Optogenetic stimulation at substantially higher frequencies would have been filtered by the kinetics of the ChR2 (~10 ms decay time; Mattis et al., 2011) and the PV-principal neuron synapse (~15 ms rise and decay times (Packer and Yuste, 2011), and would have reduced the power in the relevant portion of the spectrum. Optogenetic stimulation was delivered on a random subset of trials (33 – 50%) with the phase of the 25 ms binning on each trial randomized with respect to the visual stimulus onset.

A first-order Wiener kernel was calculated from the optogenetic stimuli for trials that ended with a hit or a miss. Data from different animals were combined by normalizing the high level of the binary optogenetic power to 1. For the analysis of white noise optogenetic stimulation, only sessions with a low mean power (≤0.25 mW) were considered, and we limited the analysis to animals that contributed at least five sessions with optogenetic stimulation. Because activation of V1 PV+ neurons reliably impairs visual perception (Glickfeld et al., 2013; Cone et al., 2019, 2020; Jin and Glickfeld, 2019), we further required that the optogenetic stimulation produced an average decrement in d′ averaged across all sessions of ≥0.10. Of 12 mice tested, seven provided usable data (four female), whereas the other mice did not show an appreciable effect of optogenetic stimulation on reducing behavioral d′. No mice showed an increase in d′ because of PV+ neuron stimulation, in accordance with previous data showing PV+ neurons cannot facilitate detection when stimulated (Cone et al., 2019). Three of the seven included mice were used for both contrast steps and contrast ramps (contrast steps: 7 mice, median 25 sessions, range 7–64 sessions; contrast ramps: 3 mice, 9, 30, and 65 sessions). Confidence intervals were generated using a bootstrap procedure with 10,000 draws with replacement.

For the primary analysis, the optogenetic stimulus profiles from hit and miss trials were normalized, aligned to the onset of the visual stimulus, profiles from miss trials were inverted and then averaged for all trials (stepped contrast: 15,735 hit trials, 15,887 miss trials; ramped contrast: 8693 hit trials, 7678 miss trials). Kernels were low-pass filtered with a corner frequency of 90 Hz to eliminate noise beyond the frequency range of the stimulus.

In a separate analysis, we computed a neuronal-behavioral kernel (NBK) after aligning the optogenetic stimuli to the onset of behavioral responses (see Fig. 5*C*,*D*), which reveals neuronal contributions that were temporally aligned with the response. We also computed an NBK after stretching the time between stimulus onset and reaction time in each trial to a fixed interval, which would reveal neuronal contributions that occurred partway between stimulus onset and behavioral response. Finally, we computed an NBK using optogenetic stimuli aligned to false alarms to determine whether those errors are associated with optogenetically driven fluctuations in spike in V1 (see Fig. 5*E*,*F*).

To examine second order effects in the optogenetic stimulation, we constructed a correlation matrix for the optogenetic stimuli during the relevant period (±400 ms from visual stimulus onset) to look for temporal pairings of high- or low-level optogenetic stimulation that were associated with consistent changes in behavior. Because this analysis yielded >300,000 statistical tests, we controlled for the false discovery rate using the method of Benjamini and Hochberg (1995), using a q value threshold of 0.05.

Electrophysiological recordings and analysis. We recorded extracellularly from V1 in awake, passively viewing, head-fixed mice using multisite silicon probes (32-site model 4 × 8–100–200–177, NeuroNexus) in 10 recording sessions in five mice (one female). All mice were experimentally naive. Before recording sessions, mice were surgically prepared with headposts and optical windows, mapped for retinotopy, and injected with ChR2 as described above.

Electrophysiology sessions occurred >4 weeks after injection. Electrodes were electroplated with a gold solution mixed with carbon nanotubes (Keefer et al., 2008; Ferguson et al., 2009) to impedances of 200–500 kΩ. Mice were anesthetized with isoflurane (1.2–2% in 100% O_2) and head fixed. A gamma-corrected visual display was positioned in the visual hemifield opposite the recording site (~10 cm viewing distance). The eyes were kept moist with 0.9% saline throughout the session. We visualized ChR2-expressing areas of V1 by imaging tdTomato fluorescence with a fluorescence microscope and camera (Zeiss). The cranial window was then removed and linear multielectrode arrays lowered into V1 through a slit in the dura. We then positioned an optic fiber above the cortex at a distance comparable to that used during behavioral experiments (1.0–1.5 mm). The craniotomy was then covered with 3% agar (MilliporeSigma) dissolved in aCSF (Tocris Bioscience). The agar was covered with silicone oil to prevent it from drying out. After a 1 h recovery period, anesthetic was removed, and we waited at least an additional hour before recording.

Delivery of stimuli and data acquisition was computer controlled. Concurrent visual and optogenetic stimuli were similar to those used during behavioral experiments (stepped contrast stimuli, a Gabor patch with SD 13°; ramped contrast stimuli, full screen grating 500 ms duration). We recorded >100 repetitions of each stimulus condition (visual stimulus, visual stimulus plus white noise optogenetic stimuli).

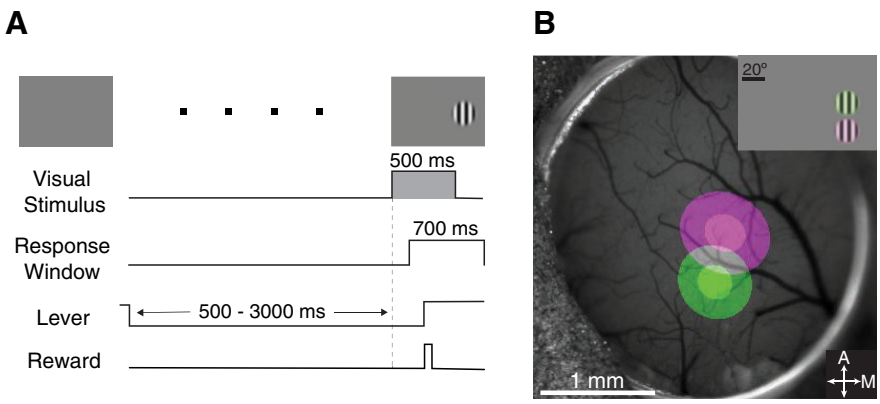

Figure 1. Visual detection task. ***A***, Trial schematic of the contrast detection task. The mouse was required to release a lever shortly after a small Gabor appeared on the display. The Gabor appeared at a random time in each trial. In some sessions the visual stimulus was a contrast step (light gray) that lasted for 500 ms, whereas in other sessions, the visual stimulus ramped from 0 to full contrast over 500 ms. ***B***, Pseudo-colored intrinsic autofluorescence responses to visual stimuli presented at two visual field locations. Green and magenta regions represent 2D-Gaussian fits of responses to stimuli at the different visual field locations (green: 25° azimuth, 0° elevation; magenta: 25° azimuth, −20° elevation; Gabor SD = 10°). Solid and transparent regions mark ±1 and ±2 SD. A, Anterior; M, medial.

Electrode signals were amplified, bandpass filtered (750 Hz to 7.5 kHz) sampled around threshold voltage crossings (Blackrock), and spikes were sorted off-line (Offline Sorter, Plexon). Analyses were done using MATLAB (MathWorks) and custom code. We recorded both single units and multiunits but did not differentiate between them because our primary interest was how optogenetic manipulations affected the V1 population.

Units were considered visually responsive to contrast steps (without optogenetic stimulation) if they exhibited a significant change in their average firing rate ($p < 0.05$; Wilcoxon signed-rank test) during the 50–150 ms after stimulus onset relative to the average firing rate during the 50–150 ms before stimulus onset. For the ramped contrast stimulus, the analysis window extended to the end of visual stimulus presentation (50–500 ms), relative to 50–500 ms before visual stimulus onset. Units were defined as optogenetically responsive if there was a significant difference ($p < 0.05$; Wilcoxon signed-rank test) in the average firing rate 50–500 ms after visual stimulus onset between trials with and without optogenetic stimulation.

We calculated the spike-triggered average (STA) optogenetic stimulus based on standard approaches (Schwartz et al., 2006). The power used for binary optogenetic stimuli was first normalized from −1 to 1. For each unit, optogenetic stimuli in windows surrounding 350 before to 100 ms after individual spikes occurred were extracted and averaged. Only units for which the minimum or maximum of the spike-triggered average exceeded 8 SEM were used in further analyses (e.g., population STA). Eliminating the inclusion criteria did not qualitatively affect our observations.

Data availability. Data are available on request.

Results

Behavioral task and virus injections

We used transgenic mouse lines that expressed Cre recombinase selectively in Par-expressing interneurons, (PV+; Hippenmeyer et al., 2005) to restrict expression of excitatory opsins to V1 PV+ interneurons (Pfeffer et al., 2013). Each mouse was implanted with a headpost and a cranial window unilaterally over V1 (Goldey et al., 2014). After recovery, they were trained to do a visual detection task in which they manipulated a lever with a forepaw to report the onset of a small Gabor stimulus that appeared on a display at a random time in each trial (Fig. 1*A*; Histed et al., 2012; Cone et al., 2019). We then mapped V1 under the cranial window retinotopically using intrinsic signals and injected the region in V1 corresponding to the training stimulus location with Cre-dependent viruses containing ChR2-tdTomato (Fig. 1*B*; Nagel et al., 2003). After allowing 2–4 weeks for virus expression, an optical fiber was fixed to the implant directly above the ChR2-expressing neurons to deliver consistent optogenetic stimulation of PV+ neurons across multiple experimental sessions.

In preliminary experiments we explored whether single, brief pulses of optogenetic activation could provide an effective approach to determining how the timing of V1 spikes contributes to visual detection. Figure 2*A* plots behavioral performance from example sessions from one mouse during which we delivered a 1 mW optogenetic stimulus to opsin-expressing V1 PV+ cells for 5 ms shortly before or after the onset of the visual stimulus. Because PV+ cells are strongly inhibitory, activating V1 PV+ impairs behavioral detection (Cone et al., 2019). As expected, optogenetic activation of V1 PV+ neurons 60–65 ms after the visual stimulus onset impaired detection of that stimulus (Fig. 2*A*, right). However, PV+ activation 140 ms before the stimulus onset caused an impairment that was just as large (Fig. 2*A*, left).

Strong PV+ activation well before the visual stimulus typically produced the largest behavioral impairments. Figure 2*B* shows the average reduction in behavioral sensitivity (measured as change in d′, see above, Materials and Methods) associated with a range of delays relative to visual stimulus onset (226 session delays, 11 mice). Unexpectedly, pulses of optogenetic stimulation delivered well before the stimulus onset had the most robust effects. A recent study using a similar task and brief optogenetic inhibition of mouse V1 also observed significant changes in detection threshold when optogenetic stimulation was delivered before the visual stimulus, corroborating this effect (Goldbach et al., 2021). Although it is conceivable that V1 spikes occurring long before stimulus onset make the greatest contribution to behavioral detection, that is not expected from conventional strategies for decoding V1 spikes. Instead, it suggests either persisting local circuit disarrangement caused by the optogenetic stimulation or that the optogenetic stimulation disrupted the behavioral state to impair task performance. Either possibility would preclude the use of optogenetic stimulation for a precise assessment of the role of spike timing in stimulus detection. To avoid these issues, we turned to using much lower optogenetic powers that would allow V1 circuitry to remain closer to its natural operating range. This weak optogenetic stimulation dictated the use of the more efficient and unbiased sampling that can be provided by white noise stimulation.

White noise optogenetic stimulation was presented to V1 PV+ neurons throughout a randomly selected subset of trials. Because the onset and offset of ChR2 activation take tens of milliseconds (Mattis et al., 2011), we constructed the stimulus for each trial by randomly assigning zero or full power to each 25 ms trial interval (binary white noise). Behavioral outcomes on trials with white noise optogenetic stimulation were used to construct an NBK (see above, Materials and Methods for details). Figure 3 illustrates the analysis for an individual session that produced an uncommonly clear kernel. We first extracted all stimulated trials

that ended in a successful detection (hit) or a failure to detect (miss; Fig. 3*A*). For the primary analysis, we separated hit and miss trials, aligned the trials on the time of their visual stimulus onset, and normalized the high binary optogenetic stimulus waveform for each trace to one to account for different powers used across mice with different levels of virus expression (median power 0.15 mW, IQR = 0.09–0.25 mW; Fig. 3*B*,*C*). The visual-stimulus-aligned optogenetic waveforms could then be averaged to produce kernels separately for the hit and miss trials. Figure 3*B* (bottom) shows the hit kernel for this session. The average stimulation remains near the mean normalized power (0.5), but there is a prominent dip of ~50 ms after stimulus onset. This indicates that reduced optogenetic stimulation of V1 PV+ neurons during this period was associated with a greater probability of behavioral stimulus detection. A negative peak is expected because lower optogenetic power would reduce inhibition onto excitatory neurons in V1. Figure 3*C* shows that the miss kernel has a somewhat smaller positive peak around the same time, correspondingly indicating that increased optogenetic stimulation during this period was associated with lower probability of stimulus detection. Asymmetric hit and miss kernels can arise in several ways, in particular if behavioral performance is near saturation on unstimulated trials during a session. Across all sessions, hit and miss kernels were essentially symmetric (see below).

We combined the data from each session into a single NBK by averaging the mean-subtracted normalized optogenetic waveforms from all trials after inverting those from miss trials (first-order Wiener kernel; Fig. 3*D*). This kernel represents the linear temporal weighting that describes how optogenetically activating V1 PV+ neurons at times relative to the visual stimulus onset relates to behavioral detection of that stimulus (De Boer and Kuyper, 1968). A normalized power of zero corresponds to the presence or absence of the optogenetic stimulus having no impact on the animals ability to detect the visual stimulus. The large negative peak in Figure 3*D* ~50 ms after visual stimulus onset corresponds to reduced optogenetic stimulation at this time making the animal more likely to detect the visual stimulus. The smaller peaks at other times were not consistent across sessions.

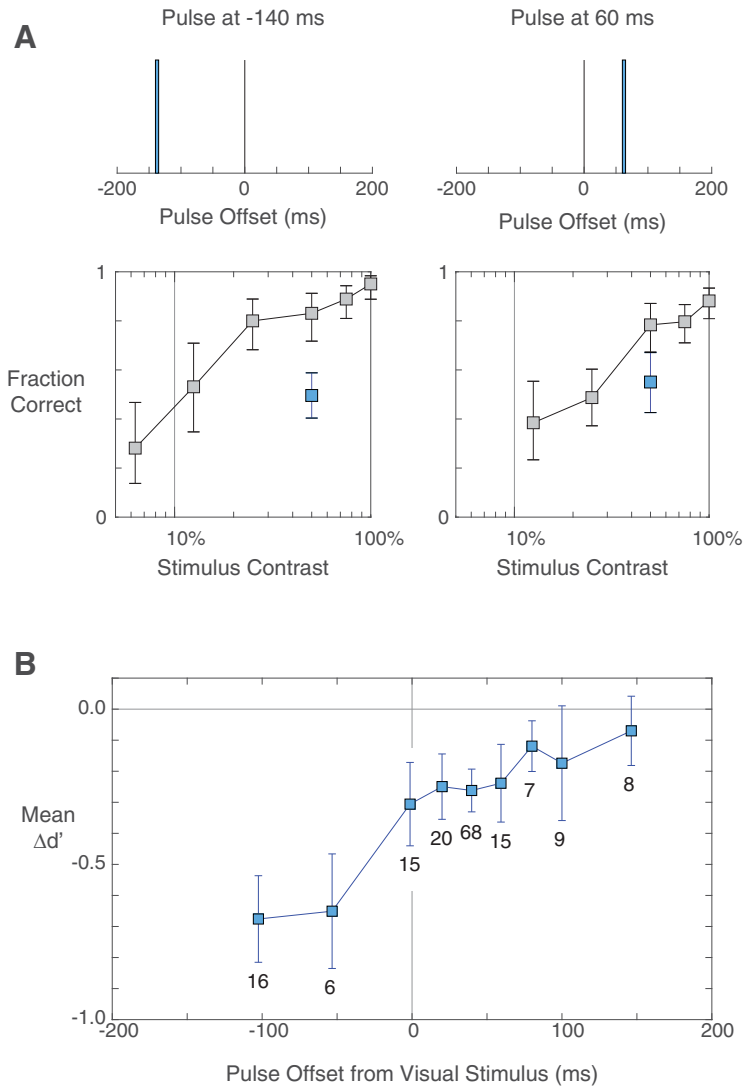

Figure 2. Behavioral effects of brief individual pulses of optogenetic stimulation of V1 PV+ neurons at different times relative to visual stimulus presentation. ***A***, Example sessions during which 5 ms 1 mW optogenetic stimulus was delivered 140 ms before (top left) or 60 ms after (top right) the onset of randomly timed 50% contrast Gabor stimuli. Detection of the stimulus (bottom) was impaired by optogenetic stimulation (blue points) relative to trials with no optogenetic stimuli (gray points), whether the PV+ activation occurred before or after the visual stimulus appeared. ***B***, Behavioral effects of optogenetic stimulation averaged over 226 session delays from 11 mice, measured as change in d′ between unstimulated and stimulated trials. Unexpectedly, the greatest impairments were associated with brief stimulation that occurred before stimulus onset. Numbers show how many sessions contributed to each value. Error bars are ±1 SEM.

Significant NBKs were not obvious in most individual sessions (which typically included 100–300 stimulated trials), but data from different sessions and animals can be combined. Figure 4 shows across-session average NBKs individually for seven mice for which optogenetic stimulation decreased d′ by an average of ≥0.10 across sessions (see above, Materials and Methods). Plots are arranged from largest to smallest d′ decrement. The prominence of the optogenetic kernel covaries with size of change in behavioral d′ caused by the optogenetic stimulus. Variance in the kernel size and change in d′ likely arises from factors such as the strength of opsin expression over the course of data collection and the number of opsin-expressing neurons effectively illuminated by the optical fiber. Sessions or animals lacking appreciable optogenetic effects cannot reveal the relationship between neuronal activity and behavior, but their inclusion will only reduce the magnitude and signal-to-noise of an average NBK.

Figure 5*A* combines data from all these animals to show an overall NBK (seven mice, 199 sessions). This average NBK is only slightly broader than that from the single session in Figure 3*D*, implying relatively consistent timing of effects across animals and sessions. The negative peak of the average NBK occurs 51 ms after the onset of the visual stimulus, and the NBK was significantly negative from 14 to 117 ms ($p < 0.05$, one tailed).

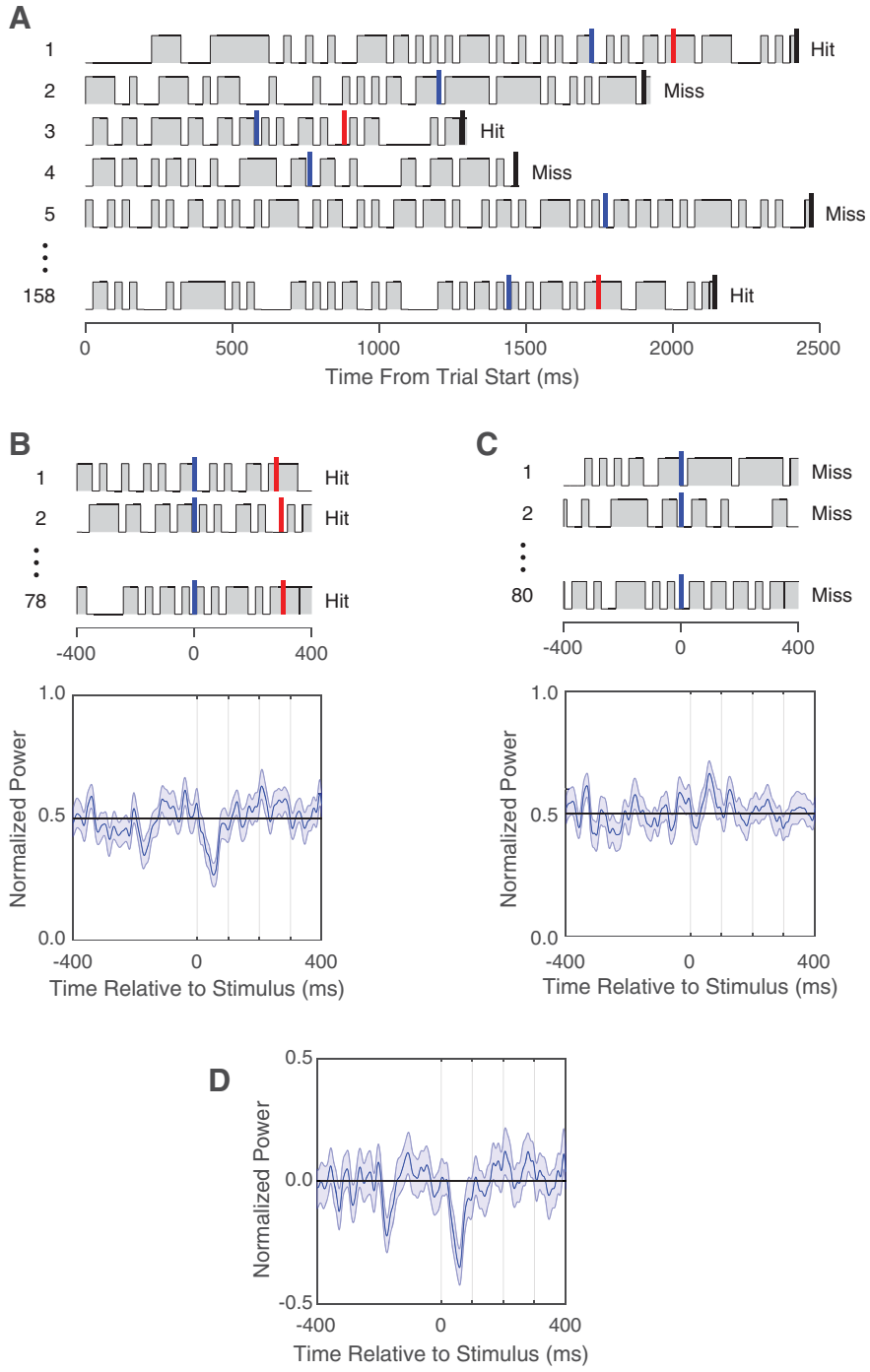

Figure 3. Construction of the neuronal-behavioral kernel. ***A***, Representative optogenetic stimulus profiles taken from individual trials in a session that included 158 trials with 0.25 mW optogenetic stimulation. For each trial, gray indicates the 25 ms periods randomly assigned for optogenetic stimulation, blue lines mark visual stimulus onset, red lines mark lever releases, and black lines mark the end of the reaction time window. Outcomes are indicated to the right of each trial. ***B***, A kernel based on hit trials was constructed by averaging the optogenetic stimulus profiles from the 78 trials with successful detections. Bottom, The average is plotted. A brief dip in the kernel ~50 ms after visual stimulus onset ($t = 0$) shows that successful detections were more likely when the optogenetic stimulation was weaker during this period. ***C***, A kernel was similarly constructed from the 80 trials on which the mouse failed to respond to the stimulus. The brief rise in the kernel ~50 ms after the visual stimulus onset shows that misses were more likely when the optogenetic stimulation was stronger during this period. ***D***, A full NBK was constructed using all trials by subtracting the mean power and inverting the optogenetic stimulus profiles from the miss trials before averaging. Bands on the plots represent ±1 SEM.

PV+ neuron stimulation before the visual stimulus or 200 ms after visual stimulus onset had no obvious effect on behavior, although the visual stimulus remained on the display until the end of the trial.

This kernel shows that V1 activity was causally linked to the behavioral response in this task and that a relatively early and short period of V1 spiking contributes most to performance. The peak of the V1 NBK was ~250 ms before the peak in the reaction time distribution of the animal, which appears in the superimposed response time histogram. This brief epoch revealed with relatively weak optogenetic stimulation supports the view that the much longer lasting effects seen with much stronger powers (Fig. 2) result from perturbations that either lead to sustained circuit disruption or changes in behavioral state.

In constructing the NBK in Figure 5*A*, optogenetic stimuli were aligned to the onset of the visual stimuli ($t = 0$). We selected this alignment because we expected the neuronal response and behavioral contribution from a sensory area like V1 to be linked to the visual stimulus onset. However, other alignments are possible. In particular, an NBK can be calculated using optogenetic stimuli that have been aligned with the behavioral response for each hit trial. A response-time-aligned NBK would be a natural choice if optogenetic perturbations were delivered to motoneurons. The response-time-aligned V1 NBK (Fig. 5*C*) was much broader than the visual-stimulus-aligned NBK in Figure 5*A*, suggesting that the spikes in V1 that drive the detection of a visual stimulus are those that occur time locked to the onset of that stimulus and that most behavioral response time variability occurs in structures that lie between the V1 neurons that contribute to the behavior and the motoneurons that generate the response (Lee et al., 2016). Additionally, a V1 kernel constructed using optogenetic stimuli aligned to lever releases on trials with a false alarm revealed no significant peaks (Fig. 5*E*,*F*). This suggests that false alarms were not driven by fluctuations in V1 activity causing the animals to perceive a fictive visual stimulus but rather were driven by activity in other brain regions. This is consistent with behavioral data showing that mice cannot detect isolated activation of their V1 PV+ neurons (Cone et al., 2019, 2020). The temporally restricted effects associated with the sustained optogenetic stimulation rule out behavioral effects arising from the optogenetic stimulus causing cortical heating, direct retina stimulation, or nonspecific behavioral effects.

We additionally asked whether behavior might be affected by second-order properties of the optogenetic stimulus. For

example, was behavior affected by consistent pairings of high or low optogenetic stimulation at particular times relative to visual onset? We constructed a correlation matrix for the optogenetic stimuli during the period ±400 ms from visual stimulus onset to look for temporal pairings of high- or low-level optogenetic stimulation that were associated with consistent changes in behavior. This analysis revealed no second-order effects of optogenetic stimulation. Following a correction for false discovery rate (Benjamini and Hochberg, 1995), all time points separated by <25 ms were significantly correlated, as expected from the autocorrelation of our 25 ms binary frame rate, but none of the time points with greater separation were significantly correlated.

The relationship between neuronal activity and behavior revealed by an optogenetic kernel should be specific to the population of neurons stimulated (e.g., sensory and motor neurons will contribute to a behavior at different times), the sensory stimulus used (e.g., perturbation of V1 neurons might have less impact on detecting brightness changes than contrast changes), and task (e.g., an animal presented with simultaneous auditory and visual stimuli should show different effects from V1 perturbations depending on whether the animal is tasked with discriminating visual or auditory stimuli.). To see whether different neuronal-behavioral kernels can be readily resolved, we optogenetically stimulated V1 in some of the same mice while they detected a different visual stimulus that required longer integration.

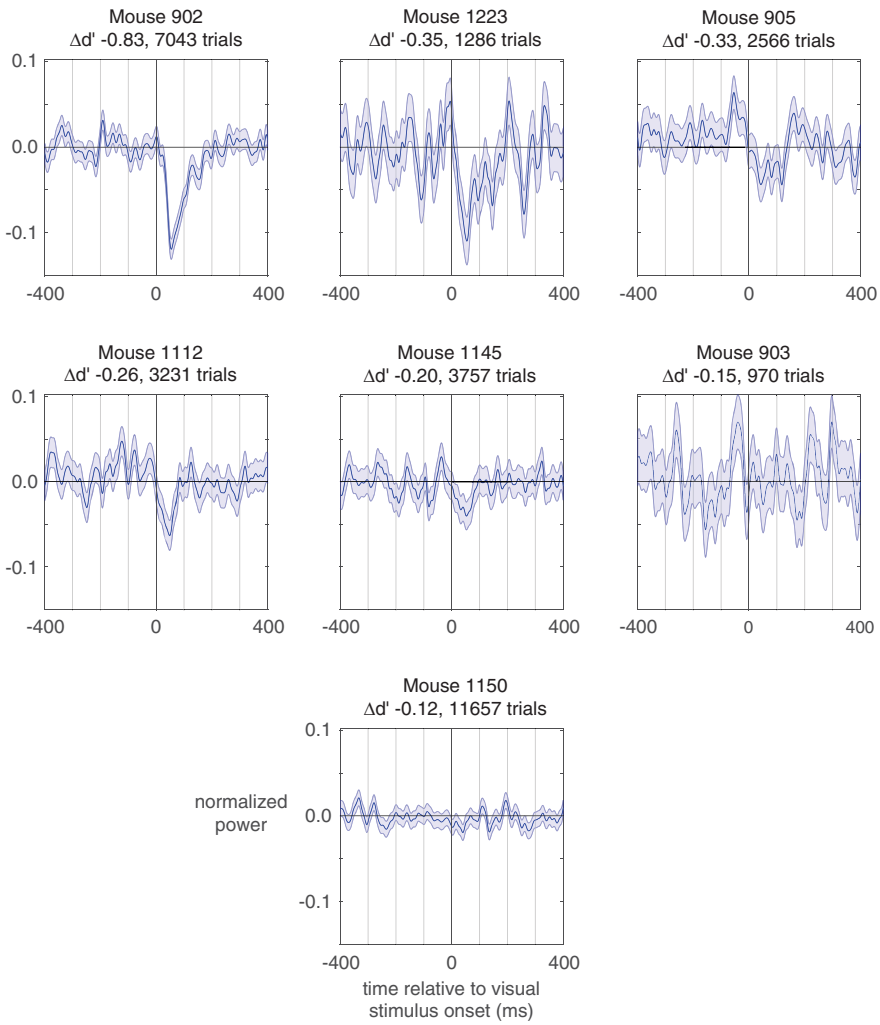

Figure 4. Neuronal-behavioral kernels for individual mice. Each plot is the neuronal-behavioral kernel aligned to the onset of Gabor contrast steps for an individual mouse. Plots are ordered by the session-averaged decrement in behavioral d′ caused by optogenetic activation of PV+ V1 neurons. The prominence of the optogenetic kernel covaries with the change in behavioral d′ caused by the optogenetic stimulus. The shaded regions demarcate ±1 SEM.

We ran separate sessions in which the contrast of the Gabor stimulus ramped linearly from 0% to full contrast over 500 ms, while keeping all other stimulus and task parameters the same. As expected, the median behavioral response time for the ramping stimulus was longer than for contrast steps (by 63 ms: 413 ms vs 350 ms; Fig. 5*A*,*B*, histograms). The negative peak of the NBK for ramped Gabors (Fig. 5*B*, green trace) was noisy but was similarly delayed relative to the NBK for the contrast steps (by 83 ms: 134 ms vs 51 ms). The NBK for ramped Gabors was significantly below 0 from 97 to 187 ms ($p < 0.05$, one tailed, uncorrected). This difference shows that the NBKs derived from optogenetic stimulation can reveal small differences in the timing of contributions from a given neuronal population under different behavioral conditions.

Comparing neuronal behavioral kernels and neuronal activity in V1

The early occurrence of the NBKs suggest that behavior depends on the spikes that occur shortly after stimulus onset. However, the timing of the kernel cannot be compared directly with spike timing in V1 because the effects of optogenetic stimulation on V1 spiking can be delayed relative to the optogenetic stimulus. PV+ cell spiking will lag the optogenetic stimulus by some amount, and there will be delays in the propagation of inhibitory signals to principal cells (Packer and Yuste, 2011) and potential polysynaptic network effects that will unfold in V1 over a longer time course (Li et al., 2019). The relevant delays can be captured by recording the responses of V1 neurons to optogenetic white noise stimulation. An STA of a white noise stimulus provides the impulse response of a spiking neuron (Bryant and Segundo, 1976), and the aggregated STA of V1 neurons provides the overall response of V1 spiking to an impulse of optogenetic PV+ stimulation, capturing the relevant delays in changes in spiking.

We made acute electrophysiological recordings from single and multiunit sites in V1 using multielectrode arrays in five awake mice that expressed ChR2 in PV+ V1 neurons, collecting responses to stepped or ramped Gabor stimuli in different datasets (see above, Materials and Methods). Visual responses from mouse V1 neurons are characteristically weak (Glickfeld et al., 2013; Siegle et al., 2019), and because we recorded simultaneously from many neurons, the stimuli were not optimal for most units. When the stepped Gabor was presented, 38% of units (24/63) were significantly excited, and 3% (2/63) were significantly inhibited ($p < 0.05$, Wilcoxon signed-rank test). The median

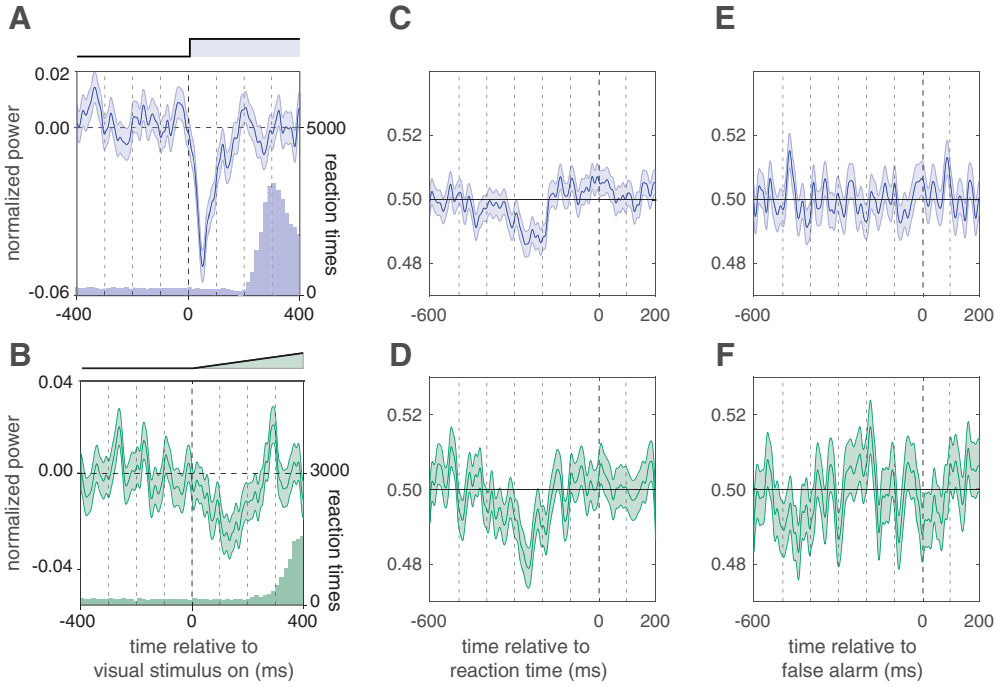

Figure 5. Neuronal-behavioral kernels identify the critical moments of V1 spiking underlying visual stimulus detection. ***A***, The NBK for detecting rapid appearance of a Gabor stimulus (t = 0) constructed combining trials with optogenetic stimulation from 199 sessions from seven mice. The superimposed histogram shows a portion of the reaction time distribution. ***B***, Same as ***A***, except for sessions in which the visual contrast ramped from 0% to full contrast over 500 ms (104 sessions, 3 mice). The peaks of both the kernel and the reaction time distribution are later than with the contrast step. ***C***, ***D***, NBKs for Gabor contrast steps and ramps computed using hit trials after aligning the optogenetic stimuli on lever release rather than stimulus onset. This alignment results in a broader kernel, suggesting that timing after stimulus onset is more relevant for determining whether V1 activity contributes to behavior. ***E***, ***F***, NBKs for Gabor contrast steps and ramps computed after aligning the optogenetic stimuli to lever releases on false alarm trials. No large deflections are evident, suggesting that V1 is not strongly involved in producing false alarms. Bands on the plots represent ±1 SEM.

response across all units was 0.6 spikes/s ($p < 10^{-6}$, Wilcoxon signed-rank test). A different set of neurons was tested with ramped Gabors, for which 49% of units (34/70) were significantly excited, and 14% (10/70) were significantly inhibited ($p <$ 0.05, Wilcoxon signed-rank test). The median response to ramped Gabors across all units was 0.4 spikes/s ($p < 10^{-5}$, Wilcoxon signed-rank test). On a fraction of trials, a white noise optogenetic stimulus was delivered before, during, and after the Gabor, with a mean power in the range used in the behavioral studies (0.25 mW). Among individual units that were significantly modulated by optogenetic stimulation, most were inhibited (stepped Gabors: 22/33 inhibited, 11/33 excited; ramped Gabors: 40/53 inhibited, 13/53 excited, all p values < 0.05; see above, Materials and Methods), but the low-power optogenetic stimulus caused only a modest reduction in spiking (stepped Gabors: median −0.14 spikes/s, IQR −0.42 to +0.10, n = 63; ramped Gabors: median −0.27 spikes/s, IQR −1.3 to +0.10, n = 70; step, ramp p values both < 0.05, both Wilcoxon signed-rank test).

The STA is a reverse correlation of the optogenetic stimuli aligned to the occurrence of individual spikes (at t = 0). We measured significant STAs in 41/70 units that were tested (see above, Materials and Methods for inclusion criteria). The population STAs shown in Figure 6, *A* and B, thus reveal the average delays between optogenetic stimulation and changes in spiking. Figure 6*A* shows the aggregate STA of the three V1 units that were excited by optogenetic stimulation (putative PV+ cells expressing ChR2). These units spiked with short latencies (<10 ms) following increments in the optogenetic stimulus power. The STA has a large positive peak 2 ms before spikes occurred, showing that putative PV+ cells responded with very short latency following a step in the optogenetic stimulus power. This STA peak is artifactually widened by the pulse width that we used for the optogenetic stimulus, which broadened peaks by 25 ms, which is why the positive peak extends to times after the spike time (t = 0), when optogenetic stimulation could have no influence on spiking.

The average STA for the remaining V1 units that were not directly excited by optogenetic stimulation (e. g., putative principal neurons, n = 38) is plotted in Figure 6*B*. It has a distinctly different form and shows that most V1 neurons tend to spike ~12 ms after a decrease in optogenetic power. An earlier positive peak around −80 ms implies there is a rebound effect, so a spike is more likely if it is preceded by above-average PV stimulation at this time. The timing of the negative peak of the STA indicates that the dominant effects of optogenetic PV stimulation (such as the NBK) on overall V1 spiking lag the optogenetic stimulus by only 12 ms.

The average responses of V1 neurons to stepped and ramped Gabors are shown in Figure 6, *C* and *D*. Gray bands mark the periods during which the associated NBK was greater than half-maximal [i.e., full-width at half-maximum (FWHM)], after adding 12 ms delay of the optogenetic effects on spiking (Fig. 6*B*). Given the approximately triangular shape of the NBKs, the FWHMs include ~75% of the spiking changes that influenced behavior (step, 43–105 ms; ramp, 110–195 ms). Although the FWHMs are nonoverlapping, both include the rising edge and earliest portions of their respective peristimulus time histograms, indicating that the earliest portion of the V1 response contains the spikes that contribute most to the behavioral response. Spikes in the later portions of the responses have far less influence in driving behavioral responses.

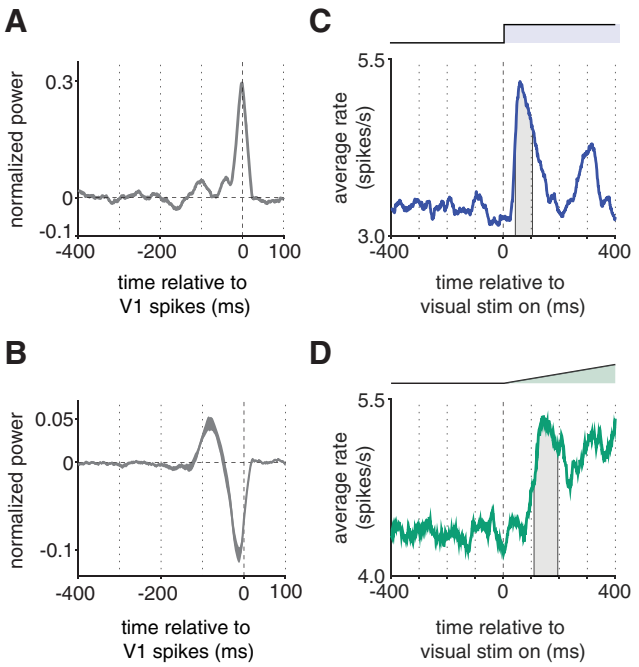

Figure 6. V1 spike-triggered average optogenetic stimuli and delay-corrected effects of neuronal-behavioral kernels on V1 spiking. Optogenetic stimulus profiles before and after V1 spikes were aligned and averaged for V1 units to calculate an STA optogenetic stimulus. Only data from cells that met inclusion criteria are shown (41 of 70 units, see above, Materials and Methods). ***A***, The gray trace depicts the STA averaged from three putative PV+ units. Spikes immediately followed positive deflections in optogenetic stimuli. ***B***, Same as in ***A***, except for the remaining 38 putative-principal V1 cells. ***C***, The blue trace represents the population response to the stepped onset of a Gabor stimulus (63 V1 units). The gray trace marks the period during which the neuronal-behavioral kernel (Figure 4*A*,*B*) exceeded FWHM, after offsetting the kernel to account for the average delay between optogenetic stimulation and V1 spiking (Fig. 6*B*). ***D***, Same as ***C***, except for Gabor contrast ramps (70 V1 units). Line widths represent 95% CIs.

Discussion

White noise sensory stimuli have long been used to study information transfer across multiple stages in the nervous system (Marmarelis and Naka, 1972; Eggermont et al., 1983; DiCarlo et al., 1998; Neri and Heeger, 2002; Schwartz et al., 2006). White noise optogenetic stimulation has recently been used to examine neuronal contributions in invertebrates as they engage in natural behaviors but with temporal modulations at 4 Hz or slower (Hernandez-Nunez et al., 2015; Porto et al., 2019). We took advantage of the fast and potent inhibition PV+ interneurons exert on local neurons in the cerebral cortex (Packer and Yuste, 2011) to use optogenetic white noise stimulation to test which moments of spiking in mouse V1 are most important for driving detection of a visual stimulus. We obtained neuronal-behavioral kernels showing that only spikes occurring within the first ~100 ms of a V1 response contribute strongly to detection. Our results are consistent with previous experimental work using sustained opsin stimulation (Resulaj et al., 2018) but provide a complete spike weighting function that is corrected for the delays inherent in optogenetic stimulation.

The outsized importance of the earliest stimulus-evoked spikes in primary sensory areas has long been inferred based on the presence of fully developed, strong stimulus selectivity at the very start of neuronal responses and complementary modeling studies examining the theoretical performance of early spikes (Tovée, 1994; Bair, 1999; VanRullen and Thorpe, 2002; Chase and Young, 2007). Dependence on a relatively small proportion of early spikes in a sensory response is consistent with visual capabilities such as fine discrimination of faces that are masked after ~50 ms of viewing (Lehky, 2000) and responses in demanding visual categorization tasks being completed in ~120 ms (Kirchner and Thorpe, 2006). Other studies have similarly pointed toward the earliest spikes being preferentially used in a variety of tasks and areas (Oram and Perrett, 1992; Müller et al., 2001; Chen et al., 2008; Mukherjee et al., 2019). Shriki et al. (2012) found that visual stimulus orientation could be decoded using only the timing of the first spikes from small populations of neurons. Given the wide range of response latencies seen for neurons within individual cortical visual areas (Schmolesky et al., 1998), neurons with the longest response latencies (typically near the surface of cortex; Best et al., 1986; Maunsell and Gibson, 1992; Raiguel et al., 1999) might contribute relatively little to fast behavioral detection.

It is important to recognize that the kernels we measured represent upper bounds on the intervals over which V1 spikes drive behavior. The 25 ms framing of our optogenetic stimulus artificially broadens the kernels and STAs. The peaks in our plots could correspond to actual functions that are as much as 50 ms narrower at their base. Future experiments could address this potential broadening by using opsins with faster dynamics (ChETA, Chronos; Gunaydin et al., 2010; Klapoetke et al., 2014), although no existing opsins approach 1 ms resolution. Alternatively, substantially larger datasets might support analytical methods that compensate for the broadening (e.g., deconvolution).

White noise optogenetic stimulation offers many advantages for exploring how specific brain structures and cell types contribute to behavior. Because it combines trials across different sessions and animals, relatively weak stimulation can be used, allowing the brain to remain close to its natural operating state. Because the stimulus is present throughout the trial, it efficiently samples the entire perceptual/behavioral cycle in an unbiased way. White noise stimulation can also simultaneously capture the full dynamics of the neuronal contributions from 0 Hz to the limits imposed by the dynamics of the opsin and/or the Nyquist frequency of the white noise. The relatively modest optogenetic perturbations that we used with the white noise approach meant that brain circuits remained close to their normal operating range, but it meant that we needed to combine data from 100 to 200 sessions. This amounts to many thousands of trials, which is a considerable investment in time and effort. Nevertheless, this number is similar to the number of trials reported in typical trained nonhuman primate neurophysiology study (e.g., Ghosh and Maunsell, 2021).

Because each NBK is specific to a particular task (i.e., stimulus-response combination), the presence, timing, and magnitude of a kernel can provide insights into whether, when, and how much particular neurons contribute during the execution of particular behaviors. The relative timing of kernels in different brain structures during a given task can provide direct evidence regarding functional relationships between spiking in different circuit elements. For example, even if kernels span tens of milliseconds, and their breadth is limited by opsin and circuit dynamics, the timing of the peaks or centers of mass of kernels in different structures might be distinguished with millisecond precision, which could potentially serve for detecting the ~5 ms increase in neuronal response latencies seen between successive levels of cortical processing (Mitzdorf and Singer, 1979). These

and other applications suggest that white noise NBKs can provide a powerful tool for exploring circuit-level contributions to behavior.

References

Andermann ML, Kerlin AM, Roumis DK, Glickfeld LL, Reid RC (2011) Functional specialization of mouse higher visual cortical areas. Neuron 72:1025–1039.

Bair W (1999) Spike timing in the mammalian visual system. Curr Opin Neurobiol 9:447–453.

Benjamini Y, Hochberg Y (1995) Controlling the false discovery rate: a practical and powerful approach to multiple testing. J Roy Stat Soc B Met 57:289–300.

Bernstein JG, Boyden ES (2011) Optogenetic tools for analyzing the neural circuits of behavior. Trends Cogn Sci 15:592–600.

Best J, Reuss S, Dinse HRO (1986) Lamina-specific differences of visual latencies following photic stimulation in the cat striate cortex. Brain Res 385:356–360.

Bryant HL, Segundo JP (1976) Spike initiation by transmembrane current: a white-noise analysis. J Physiol 260:279–314.

Chase SM, Young ED (2007) First-spike latency information in single neurons increases when referenced to population onset. Proc Natl Acad Sci U S A 104:5175–5180.

Chen Y, Geisler WS, Seidemann E (2008) Optimal temporal decoding of neural population responses in a reaction-time visual detection task. J Neurophysiol 99:1366–1379.

Cone JJ, Scantlen MD, Histed MH, Maunsell JHR (2019) Different inhibitory interneuron cell classes make distinct contributions to visual contrast perception. eNeuro 6:ENEURO.0337-18.2019.

Cone JJ, Bade ML, Masse NY, Page EA, Freedman DJ, Maunsell JHR (2020) Mice preferentially use increases in cerebral cortex spiking to detect changes in visual stimuli. J Neurosci 40:7902–7920.

De Boer E, Kuyper P (1968) Triggered correlation. IEEE Trans Biomed Eng 15:169–179.

DiCarlo JJ, Maunsell JHR (2005) Using neuronal latency to determine sensory-motor processing pathways in reaction time tasks. J Neurophysiol 93:2974–2986.

DiCarlo JJ, Johnson KO, Hsiao SS (1998) Structure of receptive fields in area 3b of primary somatosensory cortex in the alert monkey. J Neurosci 18:2626–2645.

Eggermont JJ, Johannesma PIM, Aertsen AMHJ (1983) Reverse-correlation methods in auditory research. Q Rev Biophys 16:341–414.

Ferguson JE, Boldt C, Redish AD (2009) Creating low-impedance tetrodes by electroplating with additives. Sens Actuators A Phys 156:388–393.

Glickfeld LL, Histed MH, Maunsell JHR (2013) Mouse primary visual cortex is used to detect both orientation and contrast changes. J Neurosci 33:19416–19422.

Goard MJ, Pho GN, Woodson J, Sur M (2016) Distinct roles of visual, parietal, and frontal motor cortices in memory-guided sensorimotor decisions. Elife 5:e3764.

Gold JI, Shadlen MN (2007) The neural basis of decision making. Annu Rev Neurosci 30:535–574.

Goldbach HC, Akitake B, Leedy CE, Histed MH (2021) Performance in even a simple perceptual task depends on mouse secondary visual areas. Elife 10:e62156.

Goldey GJ, Roumis DK, Glickfeld LL, Kerlin AM, Reid RC, Bonin V, Schafer DP, Andermann ML (2014) Removable cranial windows for long-term imaging in awake mice. Nat Protoc 9:2515–2538.

Ghosh S, Maunsell JHR (2021) Single trial neuronal activity dynamics of attentional intensity in monkey visual area V4. Nat. Comm 12:2003–2017.

Green DM, Swets JA (1966) Signal detection theory and psychophysics. New York: Wiley.

Gunaydin LA, Yizhar O, Berndt A, Sohal VS, Deisseroth K, Hegemann P (2010) Ultrafast optogenetic control. Nat Neurosci 13:387–392.

Guo Z, Li N, Huber D, Ophir E, Gutnisky D, Ting J, Feng G, Svoboda K (2014) Flow of cortical activity underlying a tactile decision in mice. Neuron 81:179–194.

Haefner RM, Gerwinn S, MacKe JH, Bethge M (2013) Inferring decoding strategies from choice probabilities in the presence of correlated variability. Nat Neurosci 16:235–242.

Hernandez-Nunez L, Belina J, Klein M, Si G, Claus L, Carlson JR, Samuel ADT (2015) Reverse-correlation analysis of navigation dynamics in *Drosophila* larva using optogenetics. Elife 4:e06225.

Hippenmeyer S, Vrieseling E, Sigrist M, Portmann T, Laengle C, Ladle DR, Arber S (2005) A developmental switch in the response of DRG neurons to ETS transcription factor signaling. PLoS Biol 3:e159.

Histed MH, Maunsell JHR (2014) Cortical neural populations can guide behavior by integrating inputs linearly, independent of synchrony. Proc Natl Acad Sci U S A 111:E178–E187.

Histed MH, Carvalho LA, Maunsell JHR (2012) Psychophysical measurement of contrast sensitivity in the behaving mouse. J Neurophysiol 107:758–765.

Histed MH, Ni AM, Maunsell JHR (2013) Insights into cortical mechanisms of behavior from microstimulation experiments. Prog Neurobiol 103: 115–130.

Jin M, Glickfeld LL (2019) Contribution of sensory encoding to measured bias. J Neurosci 39:5115–5127.

Keefer EW, Botterman BR, Romero MI, Rossi AF, Gross GW (2008) Carbon nanotube coating improves neuronal recordings. Nat Nanotechnol 3:434–439.

Kirchner H, Thorpe SJ (2006) Ultra-rapid object detection with saccadic eye movements: visual processing speed revisited. Vision Res 46:1762–1776.

Klapoetke NC, Murata Y, Kim SS, Pulver SR, Birdsey-Benson A, Cho YK, Morimoto TK, Chuong AS, Carpenter EJ, Tian Z, Wang J, Xie Y, Yan Z, Zhang Y, Chow BY, Surek B, Melkonian M, Jayaraman V, Constantine-Paton M, Wong GK (2014) Independent optical excitation of distinct neural populations. Nat Methods 11:338–346.

Lee SH, Kwan AC, Zhang S, Phoumthipphavong V, Flannery JG, Masmanidis SC, Taniguchi H, Huang ZJ, Zhang F, Boyden ES, Deisseroth K, Dan Y (2012) Activation of specific interneurons improves V1 feature selectivity and visual perception. Nature 488:379–383.

Lee J, Joshua M, Medina JFF, Lisberger SGG (2016) Signal, noise, and variation in neural and sensory-motor latency. Neuron 90:165–176.

Lehky SR (2000) Fine discrimination of faces can be performed rapidly. J Cogn Neurosci 12:848–855.

Li N, Chen S, Guo ZV, Chen H, Huo Y, Inagaki HK, Chen G, Davis C, Hansel D, Guo C, Svoboda K (2019) Spatiotemporal constraints on optogenetic inactivation in cortical circuits. Elife 8:e48622.

Liu H, Agam Y, Madsen JR, Kreiman G (2009) Timing, timing, timing: fast decoding of object information from intracranial field potentials in human visual cortex. Neuron 62:281–290.

Marmarelis PZ (1978) Analysis of physiological systems: the white-noise approach. New York: Plenum.

Marmarelis PZ, Naka K-I (1972) White-noise analysis of a neuron chain: an application of the Wiener theory. Science 175:1276–1278.

Mattis J, Tye KM, Ferenczi EA, Ramakrishnan C, O'Shea DJ, Prakash R, Gunaydin LA, Hyun M, Fenno LE, Gradinaru V, Yizhar O, Deisseroth K (2011) Principles for applying optogenetic tools derived from direct comparative analysis of microbial opsins. Nat Methods 9:159–172.

Maunsell JHR, Gibson JR (1992) Visual response latencies in striate cortex of the macaque monkey. J Neurophysiol 68:1332–1344.

Mitzdorf U, Singer W (1979) Excitatory synaptic ensemble properties in the visual cortex of the macaque monkey: a current source density analysis of electrically evoked potentials. J Comp Neurol 187:71–83.

Mukherjee N, Wachutka J, Katz DB (2019) Impact of precisely-timed inhibition of gustatory cortex on taste behavior depends on single-trial ensemble dynamics. Elife 8:e45968.

Müller JR, Metha AB, Krauskopf J, Lennie P (2001) Information conveyed by onset transients in responses of striate cortical neurons. J Neurosci 21:6978–6990.

Nagel G, Szellas T, Huhn W, Kateriya S, Adeishvili N, Berthold P, Ollig D, Hegemann P, Bamberg E (2003) Channelrhodopsin-2, a directly light-gated cation-selective membrane channel. Proc Natl Acad Sci U S A 100:13940–13945.

Neri P, Heeger DJ (2002) Spatiotemporal mechanisms for detecting and identifying image features in human vision. Nat Neurosci 5:812–816.

Nienborg H, Cumming BG (2009) Decision-related activity in sensory neurons reflects more than a neuron's causal effect. Nature 459:89–92.

Nienborg H, Cohen MR, Cumming BG (2012) Decision-related activity in sensory neurons: correlations among neurons and with behavior. Annu Rev Neurosci 35:463–483.

Okazawa G, Sha L, Purcell BA, Kiani R (2018) Psychophysical reverse correlation reflects both sensory and decision-making processes. Nat. Commun 9:3479.

Oram MW, Perrett DI (1992) Time course of neural responses discriminating different views of the face and head. J Neurophysiol 68:70–84.

Packer AM, Yuste R (2011) Dense, unspecific connectivity of neocortical parvalbumin-positive interneurons: a canonical microcircuit for inhibition? J Neurosci 31:13260–13271.

Panzeri S, Petersen RS, Schultz SR, Lebedev MA, Diamond ME (2001) The role of spike timing in the coding of stimulus location in rat somatosensory cortex. Neuron 29:769–777.

Parker AJ, Newsome WT (1998) Sense and the single neuron: probing the physiology of perception. Annu Rev Neurosci 21:227–277.

Pfeffer CK, Xue M, He M, Huang ZJ, Scanziani M (2013) Inhibition of inhibition in visual cortex: the logic of connections between molecularly distinct interneurons. Nat Neurosci 16:1068–1076.

Porto DA, Giblin J, Zhao Y, Lu H (2019) Reverse-correlation analysis of the mechanosensation circuit and behavior in *C. elegans* reveals temporal and spatial encoding. Sci. Rep 9:5182.

Raiguel SE, Xiao DK, Marcar VL, Orban GA (1999) Response latency of macaque area MT/V5 neurons and its relationship to stimulus parameters. J. Neurophysiol 82:1944–1956.

Resulaj A, Ruediger S, Olsen SR, Scanziani M (2018) First spikes in visual cortex enable perceptual discrimination. Elife 7:e34044.

Sachidhanandam S, Sreenivasan V, Kyriakatos A, Kremer Y, Petersen CCH (2013) Membrane potential correlates of sensory perception in mouse barrel cortex. Nat Neurosci 16:1671–1677.

Schmolesky MT, Wang Y, Hanes DP, Thompson KG, Leutgeb S, Schall JD, Leventhal AG (1998) Signal timing across the macaque visual system. J Neurophysiol 79:3272–3278.

Schwartz O, Pillow JW, Rust NC, Simoncelli EP (2006) Spike-triggered neural characterization. J Vis 6(4):13 484–507.

Seal J, Commenges D, Salamon R, Bioulac B (1983) A statistical method for the estimation of neuronal response latency and its functional interpretation. Brain Res 278:382–386.

Shriki O, Kohn A, Shamir M (2012) Fast coding of orientation in primary visual cortex. PLoS Comput. Biol 8:e1002536.

Siegle JH, Jia X, Durand S, Gale S, Bennett C, Graddis N, Heller G, Ramirez TK, Choi H, Luviano JA, Groblewski PA, Ahmed R, Arkhipov A, Bernard A, Billeh YN, Brown D, Buice MA, Cain N, Caldejon S, et al. (2019) Survey of spiking in the mouse visual system reveals functional hierarchy. Nature 592:86–92. .

Tchumatchenko T, Malyshev A, Wolf F, Volgushev M (2011) Ultrafast population encoding by cortical neurons. J Neurosci 31:12171–12179.

Tchumatchenko T, Newman JP, Fong M, Potter SM (2013) Delivery of continuously-varying stimuli using channelrhodopsin-2. Front Neural Circuits 7:184.

Tovée MJ (1994) Neuronal processing: how fast is the speed of thought? Curr Biol 4:1125–1127.

VanRullen R, Thorpe SJ (2002) Surfing a spike wave down the ventral stream. Vision Res 42:2593–2615.

Wurtz RH (2015) Using perturbations to identify the brain circuits underlying active vision. Philos Trans R Soc Lond B Biol Sci 370:20140205.